

Design of AI-based 3.84 kW Battery Package Using Backpropagation Artificial Neural Network Algorithm for Cargo Drones

Rodi Hartono,^{1,2} Sang Min Oh,¹ Sung Won Lim,¹ Tshibang Patrick A. Kalend,¹
Jasurbek Doliev,¹ Jun Hyuk Lee,¹ and Kyoo Jae Shin^{1*}

¹Department of Artificial Intelligence Convergence, Busan University of Foreign Studies,
65, Geumsaem-ro 485 Beon-gil, Geumjeong-gu, Busan 46234, Republic of Korea

²Department of Engineering and Computer Science, Universitas Komputer Indonesia,
Jl. Dipatiukur No. 112-116, Lebak Gede, Kecamatan Cobleng, Bandung 40132, Republic of Indonesia

(Received February 1, 2024; accepted March 25, 2024)

Keywords: backpropagation artificial neural network, battery management system, battery cell balancing, charge/discharge state estimation, cargo drones, emergency transportation system

Despite limitations in payload and range, cargo drones have promising applications in emergency logistics and remote delivery. In this study, we tackle these challenges by developing a high-capacity 3.84 kW battery specifically designed for a 50-kg-payload cargo drone operating in demanding terrains. Focusing on the transport of emergency goods, we investigate key drone design aspects and details of the battery pack development, including cell selection, internal configuration, and critical circuits for cell balancing, charging/discharging, and advanced battery management. A key innovation is the integration of a backpropagation artificial neural network (BPANN) algorithm to predict the depth of discharge (DoD) and the state of charge (SoC). Research results show that BPANN offers highly accurate predictions, with error percentages as low as 0.12% for DoD and 0.02% for SoC, ensuring optimized and safe battery operation. Comprehensive field testing is carried out to evaluate the effectiveness of the proposed cell balancing strategy, robust battery management system (BMS), and BPANN implementation. We investigate the drone's performance in terms of DoD, SoC, and overall field operation with the designed battery pack and demonstrate its feasibility and potential for real-world applications.

1. Introduction

Cargo drones have become a subject of research interest in recent years, especially in the context of transporting goods to remote areas. Various types of research have been carried out to explore the potential of using drones to deliver goods to hard-to-reach locations, such as mountainous areas that are difficult to access by conventional land vehicles.^(1,2) In addition, the role of cargo drones in emergency situations, such as delivering goods to traffic accident sites

*Corresponding author: e-mail: kyoojae@bufs.ac.kr
<https://doi.org/10.18494/SAM5011>

quickly and efficiently, has also attracted the attention of researchers. The ability of drones to reach difficult locations has quickly become a promising solution to support logistical assistance in emergency situations.^(3–9) In addition, the research focus is also on the concept of drone taxis as an efficient alternative means of transportation in urban areas, opening up the potential for faster and more flexible transportation services.^(10–13)

However, challenges remain in this exciting pursuit. One of the primary hurdles lies in expanding drone capacity and range. Current cargo drones have limited payloads and flight distances, necessitating advancements in efficient batteries, lightweight yet robust structural designs, and sophisticated navigation technologies. Additionally, researchers are focusing on maintaining optimal battery performance through overcharge and over-discharge protection, and other measures to ensure the long-term health and sustainability of drone operations.

Ensuring maximum battery performance through the implementation of a robust battery management system (BMS) becomes crucial to safeguard against potentially damaging extremes such as overcharge, undercharge, excessive current, and voltage fluctuations.^(14–18) Lindemark⁽¹⁷⁾ presented a systematic approach to designing the individual voltage equalizer (ICE) for reliable battery performance. This method aims to prevent individual cells within a battery pack from being overcharged. In a bid to tackle disparities in the state of charge (SoC) between battery cells, Kelkar *et al.*⁽¹⁸⁾ undertook a comprehensive study of passive and active cell balancing methods. These imbalances can stem from various factors, such as inherent variances in cell electrochemistry that affect the charging and discharging behavior, the uneven temperature distribution within the battery pack leading to disparities in charging/discharging rates, and even subtle manufacturing imperfections that cause discrepancies in cell capacity and performance over time. By addressing these SoC imbalances, cell balancing is aimed at promoting uniform cell health, enhancing battery pack performance and lifespan, and ultimately, paving the way to safer and more reliable battery operation.

Beyond these established methods, artificial intelligence (AI) is emerging as a game-changer in battery management. By analyzing vast amounts of data from battery sensors and operational history, AI algorithms can learn complex patterns and dynamics of individual battery packs. This allows them to detect early warning signs of degradation or overcharge. AI can also tailor charging profiles to individual battery needs, maximizing lifespan and minimizing stress on the cells. This can involve adjusting charging rates on the basis of current demand and cell health. AI can continuously monitor and adapt the settings of the BMS, such as voltage and balancing thresholds, in real time to account for changing environmental conditions and battery aging. AI can improve overall efficiency by optimizing charging and discharging cycles, and minimizing energy losses.^(19–31)

In this study, our focus is to develop a high-capacity 3.84 kW battery specialized cargo drone tailored for the transport of emergency goods specifically in challenging terrains such as mountainous areas and highways. The envisioned drone is designed with a targeted payload capacity of 50 kg to convey essential supplies swiftly and efficiently to locations that are typically hard to access via conventional transportation means. A key objective is the development of a battery capacity that ensures extended drone operation time, which is critical for sustained aerial operations in emergency scenarios. To achieve this, the drone's battery pack

is equipped with a cell balancing strategy and a robust BMS, and leverages a meticulously selected backpropagation artificial neural network (BPANN) to predict the depth of discharge (DoD) and SoC, thereby ensuring effective and safe operation.

This paper is structured into five sections. In Sect. 2, we delve into the design of a cargo drone, detailing its configuration and the targeted specifications for this specific design. Section 3 is focused on the design of a 3.84 kW battery pack for the cargo drone. In this section, we comprehensively explain the cell selection and specifications for the battery pack, along with its internal configuration, the design of the cell balancing circuit, the charging and discharging circuit, and the implementation of the BPANN algorithm. In Sect. 4, we discuss the experimental setup, the obtained results, and the analysis of the BPANN-based estimations of the battery pack's DoD and SoC. Additionally, this section presents the cargo drone's field test performance for providing valuable insights into the drone's performance with the designed battery pack. Finally, Sect. 5 is a summary of the key findings and conclusions drawn from the study.

2. Design of Large Cargo Drone

This study concerns the development of a large power source for the cargo drone, a drone specifically designed for heavy transport operations. Eight electric motors are used to lift the drone with a four-arm configuration. This four-arm design with eight motors is intended to provide the following features:

- Increased control and maneuverability: The additional two motors allow for finer control over individual propellers.
- Redundancy and fault tolerance: With two extra motors, the drone can still maintain some level of control and maneuverability if one motor fails or malfunctions.
- Enhanced payload capacity: The additional thrust generated by the extra motors can potentially allow the drone to carry heavier payloads than a 4-motor drone of the same size and weight.

The implementation of the drone cargo design in this research can be seen in Fig. 1. There is a special cargo drone compartment designed to accommodate the cargo and the battery that



Fig. 1. (Color online) Detailed design and dimensions of cargo drone.

provides energy to drive the drone, taking into consideration the weight to ensure the balance of the drone. As the power source of the drone, a battery pack with lithium-polymer (LiPo) batteries is used. Table 1 shows the technical specifications of the cargo drone design in this research.

3. Design of Battery Pack for Cargo Drone

3.1 Battery pack specifications and configuration

In this research, we use a pouch battery made of LiPo material with a rated voltage and capacity of 3.7 V/16 Ah for each single battery, to be arranged into a battery pack to satisfy the design target in Table 1. The single-pouch LiPo battery specifications and the proposed configuration in a pack are shown in detail in Table 2. LiPo batteries are chosen because they have a higher energy density within a smaller footprint. Furthermore, they exhibit a lower self-discharge rate and an improved cycle life. Additionally, LiPo batteries have solid-state electrolytes, which reduce the risk of leakage and eliminate the potential for electrolyte spillage, in consideration of safety concerns associated with liquid electrolytes. Moreover, these batteries exhibit greater thermal stability-related safety hazards, which are especially crucial in high-demand applications of large cargo drones.⁽³²⁾

Table 1
Technical specifications of target cargo drone design.

Evaluation indicator (item)	Design specifications	Unit
Dimensions	$2 \times 2 \times 0.7$	m
Drone flight time	15 (no payload), 12 (12 kg), 8 (24 kg), 5 (48 kg)	min
Maximum payload	50	kg
Maximum takeoff weight	150	kg
Drone rated voltage	48	Vdc
Drone battery pack rated current	80	Ah
Drone battery pack power rated output	3.84	kW
Drone battery pack weight	35	kg

Table 2
Proposed 3.84 kW battery pack specifications and configuration.

Properties of battery pack	Details
Single cell battery type	LiPo
Single cell battery dimensions (length, width, and height)	$220 \times 7.2 \times 132 \text{ mm}^3$
Weight of single cell battery	406 g
Rated voltage of single cell battery	3.7 V
Rated capacity	16 Ah
Minimum battery voltage per cell	2.7 V
Maximum battery voltage per cell	4.2 V
Operating temperature range	-20 – $60 \text{ }^\circ\text{C}$
Average specific heat	2138 J/kg-K
Battery configuration in pack	13S5P
Battery pack dimensions (length, width, and height)	$448 \times 265.6 \times 150 \text{ mm}^3$
Battery pack rated voltage	48 V
Rated battery pack capacity	80 Ah

3.2 BMS for 3.84 kW battery pack

Designing a BMS involves crucial considerations to ensure the efficient and safe operation of the battery pack. Understanding the internal impedance differences in every cell battery in a battery pack is important in designing a BMS. These differences must be taken into account in the BMS to achieve the following:

- Balance the charging process: Actively adjust charging currents to ensure all cells reach their optimal charge levels simultaneously.
- Prevent overcharging and undercharging: Monitor each cell's voltage and current individually to avoid damaging any of them.
- Optimize performance and lifespan: Ensure all cells contribute equally to the pack's capacity and power output to maximize its overall efficiency and longevity.

3.2.1 Battery cell balancing circuit

There are several balancing methods in order to balance the battery cell. One of the predominantly used methods is passive balancing using shunt resistors. The passive balancing system, achieved through the use of shunt resistors, stands out for its simplicity within the complex landscape of the BMS. Its core purpose is to maintain a consistent energy level across every cell in a battery pack, with the resistors acting as regulators. These unassuming components redirect excess energy from cells that are fully charged, preventing overcharging and fostering a balanced state among all cells. By avoiding the need for complex control systems, this passive technique ensures cost-effectiveness and reliability. Figure 2 shows the resistive passive cell-balancing circuit used in this research.

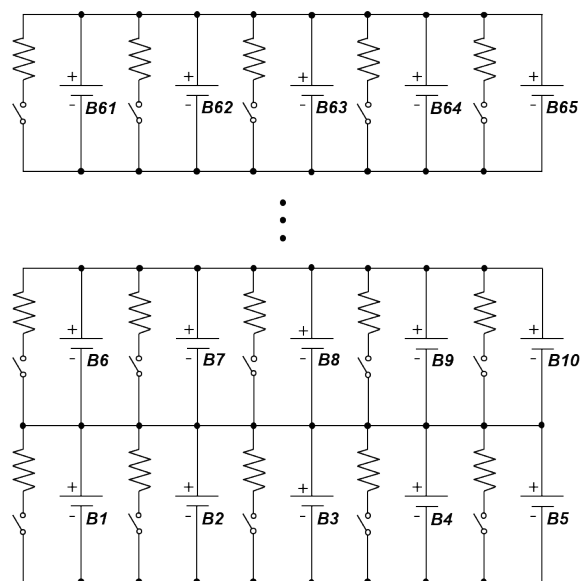


Fig. 2. Switched resistive passive cell-balancing circuit.

The proposed method for cell balancing is a variable voltage deviation approach, where the permissible voltage deviation among cells varies in accordance with the battery's operating voltage.⁽¹⁶⁾ Equation (1) represents the charge time T_{charge} required for a single cell battery to achieve a full charge, expressed using the capacity C_{batt} , SoC, and the rated charging current $I_{charged}$. T_{charge} indicates the percentage or fraction of the total charge available in the battery at a specific point in time. This equation takes into account the relationship between SoC and the charging time. In Eq. (1), SoC refers to the measure of the remaining energy in a battery relative to its fully charged capacity. For instance, a battery with a SoC of 50% means that it currently holds half of its total capacity. A SoC of 100% indicates a fully charged battery, while 0% signifies a fully discharged battery (although some batteries might maintain a minimum charge to avoid damage due to complete discharge). During charging with cell balancing, a specific cell within the battery pack is charged using a reduced current, referred to as the balancing current $I_{balance}$. The time $T_{chargebalance}$ required to fully charge this individual cell during balancing is represented by Eq. (2). This aspect illustrates how the charging time is adjusted when employing cell balancing techniques.

$$T_{charge} = \frac{C_{batt}(1 - SoC)}{I_{charged}} 3600 \quad (1)$$

$$T_{chargebalance} = \frac{I_{charged}}{(I_{charged} - I_B)} T_{charge} \quad (2)$$

Assuming a linear relationship between battery SoC and voltage, the rate of voltage change per second $V_{ratesec}$ is expressed by

$$V_{ratesec} = \frac{(V_{full} - V_{lim})}{T_{chargepack}} 3600, \quad (3)$$

where

$$T_{chargepack} = \frac{C_{batt}(1 - SoC_{pack})}{I_{charged}} 3600, \quad (4)$$

V_{full} is the full-charge voltage when charging with the rated current $I_{charged}$, V_{lim} is the minimum voltage for the balancing function, and $T_{chargepack}$ is the time needed to reach the full-charge state. Equation (5) then establishes the proper voltage difference limit between cells at a specified battery operating point, $V_{difference}$, considering these variables. Consequently, defining the voltage deviation at the battery's full charge voltage as $V_{deviation}$, Eq. (6) outlines the design of the voltage deviation threshold $V_{threshold}$ for effective balancing operations. This equation encapsulates the parameters involved in determining the threshold for voltage deviation, which is crucial for maintaining balance among cells during charging.

$$V_{\text{difference}} = (T_{\text{chargebalance}} - T_{\text{chargepack}}) V_{\text{ratesec}} \tag{5}$$

$$V_{\text{threshold}} = V_{\text{deviation}} + V_{\text{difference}} \tag{6}$$

Figure 2 shows the cell-balancing circuit implemented in every cell of the battery in a package. The switched passive resistive cell-balancing circuit control is implemented using the HY2213 integrated circuit (IC) in this research. The HY2213 IC has a precision voltage detection circuit with an overcharge detection voltage range of 4.0–4.5 V, an overcharge release voltage range of 3.8–4.5 V, and standby detection and release voltages of 2.7 V. This unit module has a low power consumption current of 2.5–3.5 uA with a standby mode of 0.5 uA ($V_{\text{DD}} = 2.7 \text{ V}$). The HY2213 IC also has a wide temperature range of -40 to $+80 \text{ }^\circ\text{C}$.⁽³³⁾ Figure 3 shows the switched resistive passive cell-balancing schematics using HY2213 IC modules and Fig. 4 shows the module of a single switched passive resistive cell-balancing fabricated board in this research. In the configuration of battery pack design 13S5P (13 batteries in series and 5 batteries in parallel) shown in Fig. 3, there is a total of 65 HY2213 ICs.

3.2.2 Charging and discharging control of 3.84 kW battery pack

In this research, the charging and discharging unit cutoff control is accomplished using an electric switched metal-oxide-semiconductor field-effect transistor (MOSFET). To read the battery pack current and its direction when charging and discharging, a current sensor is used (WCS1600). WCS1600 is a precise solution for direct current (DC) and alternating current (AC) sensing with a low-temperature drift linear hall sensor IC. It has a 9.0-mm-diameter through

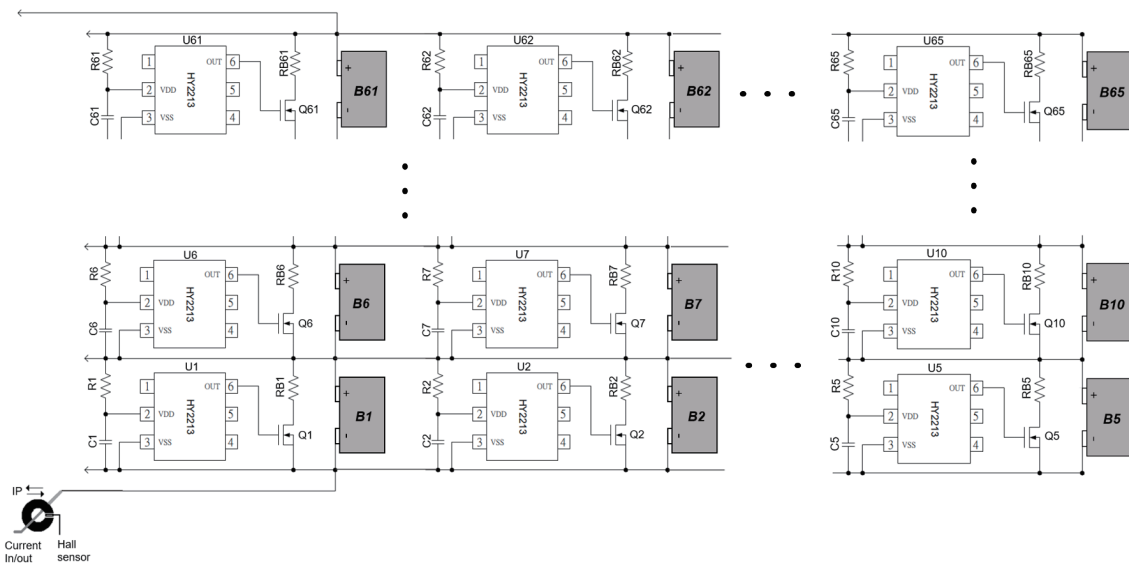


Fig. 3. Switched resistive passive cell-balancing circuit using HY2213 IC modules.

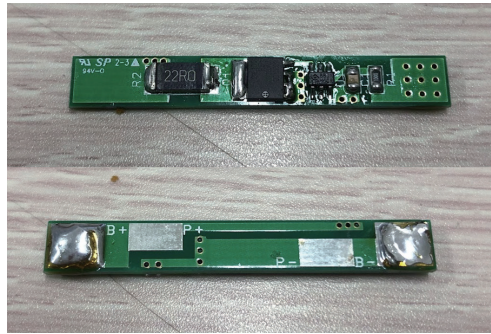


Fig. 4. (Color online) Single switched passive resistive cell-balancing fabricated board for each pouch cell.

hole and a sensitivity of 22 mV/A. The function block diagram of its application is shown in Fig. 5.

The WCS1600 sensor, as shown in Fig. 5, requires additional circuitry for effective operation. We address this requirement by designing a dedicated circuit for current sensing and amplification. For the precise control of charging and discharging cutoff, a microcontroller-based driver circuit controls the electronic switches (MOSFETs). In this research, we leverage an operational amplifier circuit for its high input impedance, low output impedance, and configurable gain characteristics. The amplifier circuit for the battery pack current and current direction sensing follows a specific design strategy.

- (1) Buffering: Sensor outputs are first fed to a buffer stage to isolate them from subsequent circuitry and prevent signal distortion.
- (2) Signal summation: An adder circuit combines the signals from multiple sensors, enabling multisensor data processing.
- (3) Voltage inversion: The output voltage is inverted.
- (4) Additional buffering: Another buffer stage ensures signal stability before feeding it to the microcontroller's ADC, reading the amplified current (analog signal).
- (5) Voltage comparison: The inverted voltage is compared to a reference voltage (2.5 V) obtained from a voltage divider. This comparison generates an output signal that indicates the direction of current flow.

Additionally, the battery voltage is sensed using a voltage divider circuit with two outputs derived from three resistors. These outputs function as low- and high-voltage results depending on the battery state (charging or discharging). The amplifier circuit for sensing the overcharge and under-discharge voltages of the battery pack follows a specific design strategy.

- (1) Buffering: Sensor outputs are first fed to a buffer stage to isolate them from subsequent circuitry and prevent signal distortion.
- (2) Differential amplification: The buffered signal enters a differential amplifier, which amplifies the difference between the maximum and minimum voltage sensor signals, improving noise rejection and extracting the desired information.
- (3) Additional buffering: Another buffer stage ensures signal stability before processing.
- (4) Signal summation: An adder circuit combines the signals from multiple sensors, enabling multisensor data processing.

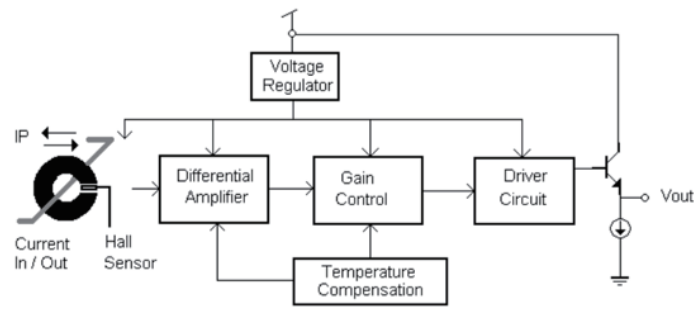


Fig. 5. WCS1600 function block diagram.⁽³⁴⁾

- (5) Voltage inversion: The output voltage is inverted.
- (6) Second buffering: Another buffer stage ensures signal stability before processing.
- (7) Threshold comparison: The inverted voltage is compared with a reference voltage obtained from a voltage divider.
- (8) Output generation: As a result of the comparison, two outputs are generated and input to the controller to read the overcharging and under-discharging voltages of the battery pack.

Figures 6 and 7 show the block diagram of BMS charging and discharging control in this research and its fabricated boards, respectively.

3.3 AI-based battery pack DoD and SoC prediction using BPANN algorithm for safe drone operation

In the previous section, we discussed the design of cell balancing and charging and discharging control to improve the performance and battery life. Cell balancing helps ensure uniform charge and discharge among cells, and charging and discharging control prevents the whole battery pack from overcharging and over-discharging. Next, understanding the remaining battery usage time is also crucial for planning flight operations to ensure the safe operation of the drones and prevent unexpected power depletion during operation. The key parameters that contribute to this understanding include DoD and SoC. DoD represents how much of the battery's total capacity has been discharged. Additionally, SoC provides insight into the remaining charge level of the battery relative to its full capacity.

There are several algorithms for estimating DoD and SoC. In this research, we used BPANN, a multilayered feedforward artificial neural network (ANN) model. The primary principle involves the forward propagation of the results, which generates an error that is then minimized and corrected through backpropagation (BP). In this algorithm, the sigmoid-type function serves as the activation function between neurons, limiting the output values to a range of 0 to 1. The BPANN structure comprises three layers: the input, hidden, and output layers. As depicted in Fig. 8, the node cells in each layer connect and interact. If the mean absolute error (MAE) between the output from the output layer and the predicted output does not meet the requirements, a reverse process with corrected weights, following the gradient descent, is initiated. Equations (7) and (8) detail the corresponding units of the ANN.

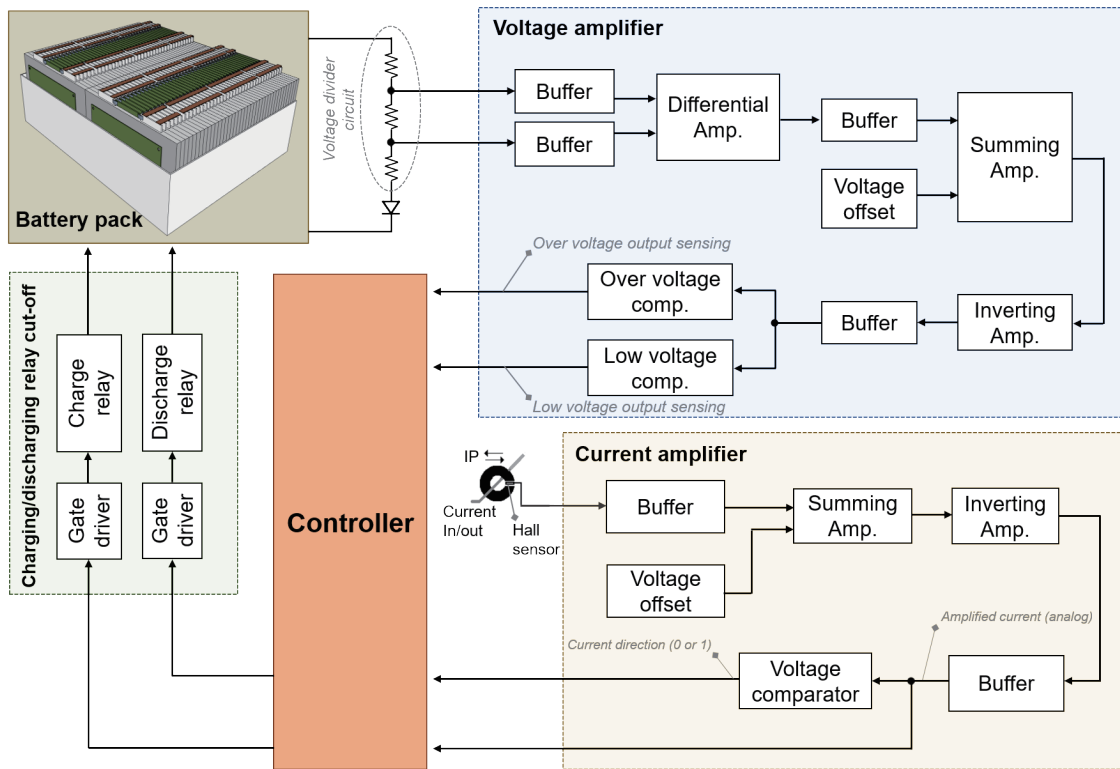


Fig. 6. (Color online) Block diagram of 3.84 kW battery pack charging/discharging control.



(a)



(b)

Fig. 7. (Color online) Fabricated boards for 3.84 kW battery pack charge/discharge control: (a) microcontroller and op-amp board, and (b) gate driver and MOSFET board.

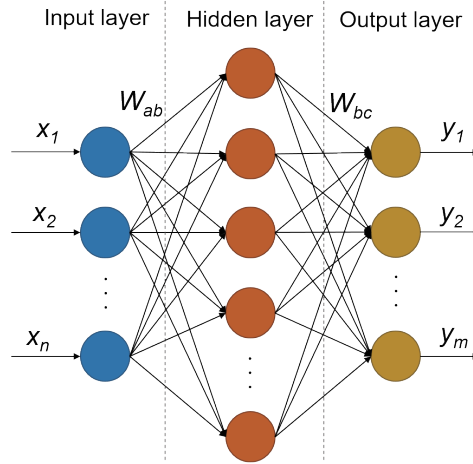


Fig. 8. (Color online) Three-layer BPANN.

$$h_a = f \left(\sum_{a=1}^n (W_{ab} x_a + \theta_a) \right) \quad b=1, 2, 3, \dots, l \quad (7)$$

$$y_c = g \left(\sum_{b=1}^l (W_{bc} p_a + \theta_c) \right) \quad c=1, 2, 3, \dots, m \quad (8)$$

Here, h_a is the hidden layer output, y_c is the output layer output, W_{ab} is the weight between the input and hidden layers, W_{bc} is the weight between the hidden and output layers, n is the number of input nodes, l is the number of hidden layer nodes, m is an output layer node, $x_a = [x_1, x_2, \dots, x_n]^T$ is the input vector, and the θ is the threshold.

Using the results from the previous feedback process, MAE is calculated as

$$MAE = \frac{1}{N} \sum_{c=1}^N (P_c - R_c). \quad (9)$$

To achieve optimal performance, the network relies on Eq. (10) to backpropagate errors, meticulously adjusting the internal weights for enhanced predictions:

$$W_{a+1} = W_a - \eta \frac{\partial E}{\partial W_a}. \quad (10)$$

Equation (10) is the weight update rule for the ANN during training. It uses the difference between predictions P_c and true values R_c across N data points to adjust the current weight W_a by a factor of the learning rate η . This iterative process, known as BP, guides the ANN towards a model that minimizes MAE, fulfilling the desired accuracy requirements. Notably, BP helps avoid getting stuck in local minima, leading to improved estimations of DoD and SoC.

To expedite the BP quest for the optimal solution, the dedicated weight and threshold correction formulae (11) through (14) are used:

$$\theta_c(L+1) = \theta_c(L) + \sigma\eta_c, \quad (11)$$

$$\theta_a(L+1) = \theta_a(L) + \sigma\eta_a, \quad (12)$$

$$W_{ab}(L+1) = W_{ab}(L) + \alpha\eta_b W_{ab} x_a, \quad (13)$$

$$W_{bc}(L+1) = W_{bc}(L) + \alpha\eta_c y_c, \quad (14)$$

where L is the learning number, x_a is the a th input signal, η_a is the BP learning rate in the hidden layer, η_c is the BP learning rate in the output layer, θ_c is the threshold in the c th layer, and σ is the threshold coefficient.

4. Experimental Results and Discussion

4.1 Accuracy analysis of BPANN for estimating DoD and SoC of battery pack

We employ BPANN to estimate the DoD and SoC of the proposed battery pack containing 65 LiPo pouch cells. The estimation process involves the following steps:

- (1) Full charge: The battery pack was charged to 100% SoC by a constant current method.
- (2) Resting period: After charging, the pack was left to rest for 30 min to stabilize.
- (3) Complete discharge: The pack was completely discharged to 0% SoC at a constant current of 40 A.
- (4) Data acquisition: During discharge, voltage, current, time, and temperature were continuously measured by the controller board.
- (5) Cycling: Steps 1–4 were repeated 150 times to create a dataset of 150 cycles.
- (6) Data processing: The collected data were transferred to a computer and preprocessed for BPANN training.
- (7) BPANN training: The BPANN model was trained with the processed data to learn the relationship between the measured parameters and DoD/SoC.
- (8) Evaluation: The BPANN-predicted DoD and SoC values were compared with the experimental measurements.
- (9) Error assessment: MAE was calculated to quantify the accuracy of BPANN predictions.

Figure 9 shows the experimental setup used to evaluate the 3.84 kW battery pack. Both charging and discharging tests were conducted, with the results displayed in Figs. 10 and 11, respectively. One complete charge and discharge cycle defines a single cycle. The initial voltage for discharge was set at 52 V with a lower limit of 41.6 V. A constant current of 40 A or a rate discharge of 0.5 C was used for discharging. As expected, owing to battery degradation, the discharge time decreased from 88.7 min at the 10th cycle to 79.3 min at the 150th cycle. For



Fig. 9. (Color online) Experimental setup for charging and discharging test of 3.84 kW battery pack: (a) 3.84 kW battery pack, (b) resistor load unit, (c) upper computer, (d) transducer, and (e) data acquisition instrument.

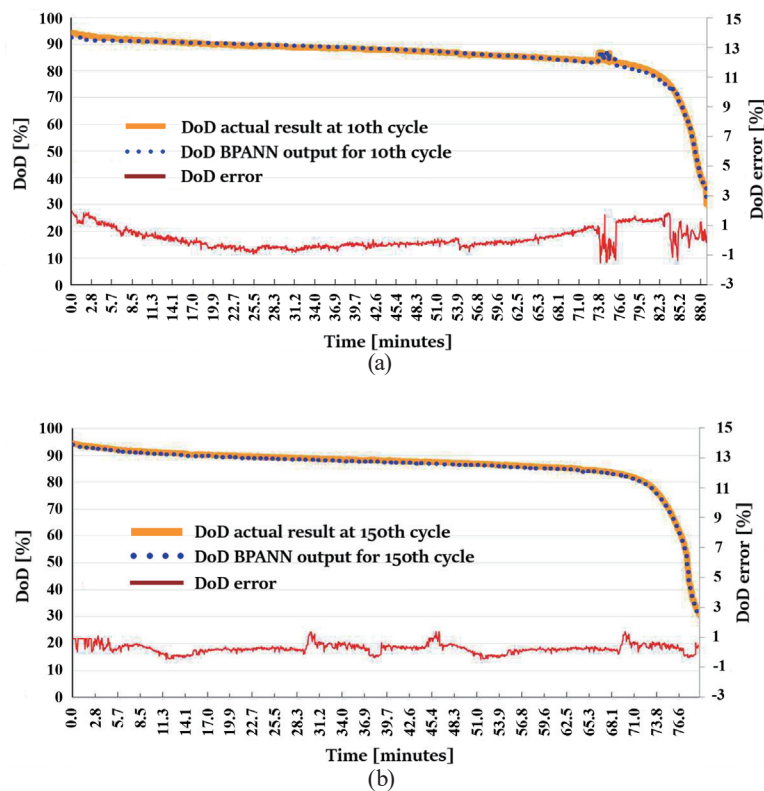


Fig. 10. (Color online) Experimental results of DoD prediction performance of BPANN and actual measurement results for (a) 10th and (b) 150th cycles.

charging, the initial voltage was set at 41.6 V, with an upper limit of 52 V. Again, a constant current of 40 A (0.5 C) was used. Initially, charging the battery took 89.3 min. Curiously, this time gradually decreased to 79.6 min by the 150th cycle. This observed change can be attributed to alterations in the battery's internal chemical reaction rate. Throughout each charge and

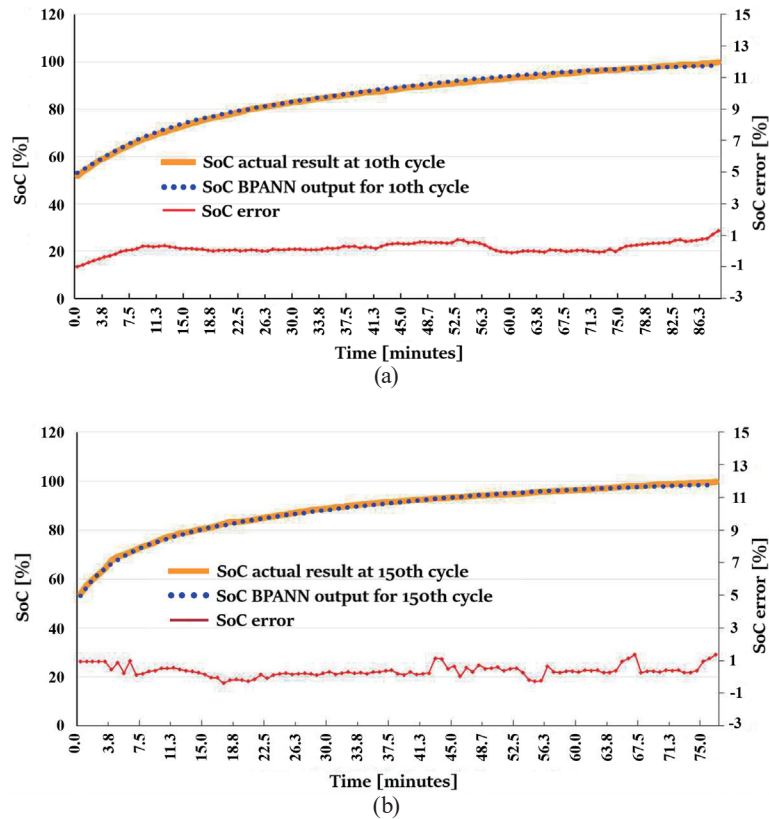


Fig. 11. (Color online) Experimental results of SoC prediction performance of BPANN and actual measurement results for (a) 10th and (b) 150th cycles.

discharge cycle, essential parameters such as current, voltage, time, and temperature were continuously recorded using sensors and microcontroller programming. These parameters are critical for calculating the DoD and SoC of the battery. The key discharge and charge experiment-related results are summarized in Tables 3 and 4, respectively, for the 10th and 150th cycles.

An actual discharge test was conducted under 0.5 C conditions for both the 10th and 150th cycles. The proposed BPANN algorithm, integrated within a battery learning model, was then applied to predict DoD from the collected data. Figure 10 shows the results of this error analysis. The predicted DoD estimates are shown with the measured experimental values. On the basis of the calculated MAE, the DoD prediction exhibits reassuringly low deviations of only 0.12% in the error prediction percentage for the 10th cycle and 0.17% for the 150th cycle. This confirms the effectiveness of the BPANN learning model for DoD estimation. Furthermore, in the experiment, a gradual decline in voltage with increasing number of discharge cycles was observed. In the 10th cycle, the battery took 88.7 min to fully discharge with a constant voltage decrease. However, at the 150th cycle, a marked voltage drop led to a faster discharge (79.3 min). This aligns well with the BPANN model predictions, demonstrating its accuracy.

Following the DoD experiment, an SoC evaluation was conducted under 0.5 C charging conditions. Similarly to DoD, actual SoC values were measured for the 10th and 150th cycles

Table 3
Operating conditions for 3.84 kW battery pack during discharge experiment.

Discharge cycle	Time (min)	Lowest voltage limit (V)	Rated voltage limit (V)	Highest voltage limit (V)	Temperature (°C)
10th cycle	88.7	41.6	48.1	52	28.2
150th cycle	79.3	41.6	48.1	52	37.2

Table 4
Operating conditions for 3.84 kW battery pack during charge experiment.

Charge cycle	Time (min)	Lowest voltage limit (V)	Rated voltage limit (V)	Highest voltage limit (V)	Temperature (°C)
10th cycle	89.3	41.6	48.1	52	28.0
150th cycle	79.6	41.6	48.1	52	32.3

and used to train the BPANN model. The predicted and measured SoC values yielded MAEs of only 0.02% in the error prediction percentage for the 10th cycle and 0.36% for the 150th cycle, indicating a close match between predictions and actual measurements. Figures 11(a) and 11(b) graphically show the predicted results with the experimental data. As seen, the results of both the DoD and SoC experiments demonstrated the BPANN model's ability to accurately predict the battery pack behavior under real-world conditions.

4.2 Cargo drone field test performance

A comprehensive field evaluation was conducted to assess the performance of the custom-designed drone battery pack under realistic operating conditions. This evaluation comprised a rigorous testing methodology for meticulously measuring the key parameters during flight trials. Figures 12(a), 12(b), and 12(c) show the real-world flight testing of the cargo drone in this research. The trials involved loading the drone without and with a representative payload of 12, 24, or 48 kg and systematically discharging the battery pack until it reached its designated voltage limit of 41.6 V. This limit was established on the basis of prior electrochemical characterization and safety considerations to ensure optimal battery health and longevity.

During each flight, comprehensive data were logged, including battery voltage, current, temperature, and drone flight parameters such as altitude, airspeed, and power consumption. Such data were meticulously analyzed to evaluate the battery pack's capacity, discharge characteristics, thermal stability, and impact on overall drone flight performance. The results of the field evaluation are summarized in Table 5. The initial design goals were fulfilled with the achieved performance metrics. The statistical analysis of the flight data confirmed stable drone operation throughout the discharge cycle, demonstrating the success of the battery pack design in meeting critical performance requirements.

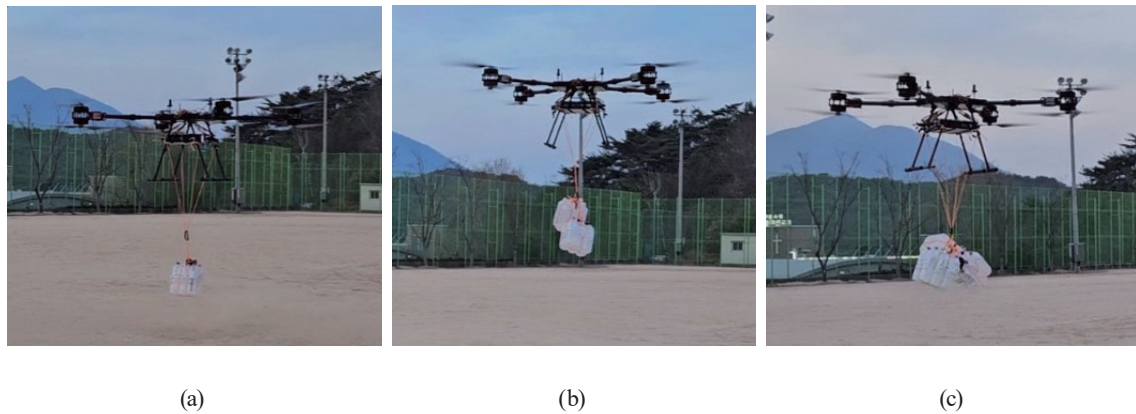


Fig. 12. (Color online) Real-world flight testing of cargo drone to assess proposed battery pack energy consumption using (a) 12, (b) 24, and (c) 48 kg payloads.

Table 5
Technical specifications for cargo drone design target and realized values.

Evaluation indicator (item)	Unit	Development target	Realization
Dimensions	m	$2 \times 2 \times 0.7$	$2 \times 2 \times 0.7$
Maximum payload	kg	50	50
Drone flight time	min	15 (no payload), 12 (12 kg), 8 (24 kg), 5 (48 kg)	15 (no payload), 12 (12 kg), 8 (24 kg), 5 (48 kg).
Drone rated discharge	C	—	4 C with no payload, 5 C with 12 kg payload, 7.5 C with 24 kg payload, and 12 C with 48 kg is 12 C
Maximum takeoff weight	kg	150	150
Drone power rated voltage	Vdc	48	48
Drone power rated current	Ah	80	80
Drone power rated output	kw	3.84	3.84
Drone total battery pack weight	kg	35	33.7

5. Conclusions

We designed and achieved a high-capacity 3.84 kW battery specifically tailored for a 50-kg-payload drone operating in demanding terrains. This novel design was focused on the transport of emergency goods, and we investigated key aspects of the drone's battery pack design, including cell selection, internal configuration, and advanced BMS. In this study, the integration of a BPANN algorithm for predicting DoD and SoC was highlighted. The results of thorough field testing validated the effectiveness of the proposed cell balancing strategy, robust BMS, and BPANN implementation. Analysis results of the drone's performance in terms of DoD, SoC, and overall field operation with the designed battery pack validated its real-world applicability. The BPANN offers highly accurate predictions, with error percentages as low as 0.12% for DoD and 0.02% for SoC. The drone achieved adaptable flight times based on payload: 15 min with no payload, 12 min with a 12 kg payload, 8 min with a 24 kg payload, and 5 min with a 48 kg payload, demonstrating its capability for diverse delivery needs.

Acknowledgments

This research was supported by Regional Innovation Strategy (RIS) through the National Research Foundation of Korea (NRF) funded by the Ministry of Education (MOE) (2023RIS-007).

References

- 1 K. M. Klinkmueller, A. J. Wieck, J. K. Holt, and A. W. Valentine: 2019 AIAA Scitech Forum (AIAA, 2019) 2285. <https://doi.org/10.2514/6.2019-2285>
- 2 D. Cvitanić: 2020 5th Int. Conf. Smart and Sustainable Technologies (IEEE, 2020) 1–4. <https://doi.org/10.23919/SpliTech49282.2020.9243807>
- 3 Y. H. Ma, T. H. Shieh, L. C. Hung, and L. C. Tsai: 2021 9th Int. Conf. Orange Technology (IEEE, 2021) 1–5. <https://doi.org/10.1109/ICOT54518.2021.9680627>
- 4 K. B. Laksham: J. Family Medicine and Primary Care **8** (2019) 342. https://doi.org/10.4103/jfmipc.jfmipc_413_18
- 5 D. Moormann: Proc. ICAO RPAS Symp. (RPAS, 2015). <https://www.icao.int/Meetings/RPAS/RPASSymposiumPresentation/Day%20%20Workshop%20%20Technology%20Dieter%20Moormann.pdf>
- 6 J. E. Scott and C. H. Scott: 2017 Proc. 50th Hawaii Int. Conf. System Sciences (HICSS, 2017) 3297–3304. <https://doi.org/10.24251/HICSS.2017.399>
- 7 D. Sivabalaselvamani, D. Selvakarhi, L. Rahunathan, G. Gayathri, and M. M. Baskar: 2021 5th Int. Conf. Electronics, Communication and Aerospace Technology (IEEE, 2021) 878–883. <https://doi.org/10.1109/ICECA52323.2021.9675859>
- 8 T. Amukele, P. M. Ness, A. R. Tobian, J. Boyd, and J. Street: Transfusion **57** (2016) 582. <https://doi.org/10.1111/trf.13900>
- 9 S. Lee and Y. J. Kwon: World J. Engineering and Technology **7** (2019) 612. <https://doi.org/10.4236/wjet.2019.74044>
- 10 A. Bajaj, B. Phillips, E. Lyons, D. Westbrook, M. Zink, V. Chandrasekar, and E. Huffman: IGARSS 2020–2020 IEEE Int. Geoscience and Remote Sensing Symp. (IEEE, 2020) 6483–6486. <https://doi.org/10.1109/IGARSS39084.2020.9324074>
- 11 H. D. Yoo and S. M. Chankov: 2018 IEEE Int. Conf. Industrial Engineering and Engineering Management (IEEE, 2018) 1216–1220. <https://doi.org/10.1109/IEEM.2018.8607829>
- 12 K. V. M. Sai Kumar, M. Sohail, P. Mahesh, and U. R. Nelakuditi: 2018 Int. Conf. Smart Systems and Inventive Technology (IEEE, 2018) 22–25. <https://doi.org/10.1109/ICSSIT.2018.8748421>
- 13 P. M. Kornatowski, M. Feroskhan, W. J. Stewart, and D. Floreano: IEEE Rob. Autom. Lett. **5** (2020) 4233. <https://doi.org/10.1109/LRA.2020.2993757>
- 14 J. Cao, N. Schofield, and A. Emadi: Battery Balancing Methods: Proc. 2008 IEEE Vehicle Power and Propulsion Conference (IEEE, 2008) 1–6. <https://doi.org/10.1109/VPPC.2008.4677669>
- 15 J. Kim, Y. Choi, S. Jeon, J. Kang, and H. Cha: IEEE Trans. Comput. Aided Des. Integr. Circuits Syst. **39** (2020) 3931. <https://doi.org/10.1109/TCAD.2020.3012790>
- 16 H. Song and S. Lee: Electronics **12** (2023) 2587. <https://doi.org/10.3390/electronics12122587>
- 17 B. Lindemark: Proc. 13th Int. Telecommunications Energy Conf. (IEEE, 1991) 196–201. <https://doi.org/10.1109/INTLEC.1991.172396>
- 18 A. Kelkar, Y. Dasari, and S. S. Williamson: 2020 IEEE Int. Conf. Power Electronics, Smart Grid and Renewable Energy (PESGRE, 2020) 1–6. <https://doi.org/10.1109/PESGRE45664.2020.9070666>
- 19 S. Jafari and Y. C. Byun: IEEE Access **10** (2022) 124685. <https://doi.org/10.1109/ACCESS.2022.3225093>
- 20 K. T. Kim, H. J. Lee, J. H. Park, G. Bere, J. J. Ochoa, and T. Kim: 2021 IEEE Energy Conversion Congress and Exposition (IEEE, 2021) 1387–1392. <https://doi.org/10.1109/ECCE47101.2021.9595404>
- 21 Vinodkumar and N. S. Singha: 2023 Int. Conf. Sustainable Emerging Innovations in Engineering and Technology (IEEE, 2023) 31–35. <https://doi.org/10.1109/ICSEIET58677.2023.10303338>
- 22 X. Tang, K. Liu, X. Wang, F. Gao, J. Macro, and W. D. Widanage: IEEE Trans. Transp. Electrification **6** (2020) 363. <https://doi.org/10.1109/TTE.2020.2979547>
- 23 W. You, Z. Qiao, X. Li, F. Feng, W. Huo, and H. Wang: 2009 2nd Int. Symp. Computational Intelligence and Design (IEEE, 2009) 400–404. <https://doi.org/10.1109/ISCID.2009.246>
- 24 K. Choi and W. Kim: IEEE Control Syst. Lett. **7** (2023) 943. <https://doi.org/10.1109/LCSYS.2022.3228946>

- 25 D. Cordova, G. Medwig, A. V. Roy, and S. Karmakar: 2021 IEEE 12th Annu. Ubiquitous Computing, Electronics & Mobile Communication Conf. (IEEE, 2021) 0298–0302. <https://doi.org/10.1109/UEMCON53757.2021.9666507>
- 26 K. J. Shin: Sens. Mater. **35** (2023) 1385. <https://doi.org/10.18494/SAM4181>
- 27 G. Suci, A. Badicu, C. Beceanu, M. S. Yumlu, Y. Kaya, K. G. Kizak, and F. Tahtasakal: 2021 12th Int. Symp. Advanced Topics in Electrical Engineering (IEEE, 2021) 1–5. <https://doi.org/10.1109/ATEE52255.2021.9425328>
- 28 A. B. Ahmad, C. A. Ooi, D. Ishak, and J. Teh: IEEE Access **7** (2019) 131. <https://doi.org/10.1109/ACCESS.2018.2885083>
- 29 D. Holeciska and A. Dineva: 2023 IEEE 17th Int. Symp. Applied Computational Intelligence and Informatics (IEEE, 2023) 000655–000660. <https://doi.org/10.1109/SACI58269.2023.10158604>
- 30 H. Feng: 2021 IEEE Int. Conf. Advances in Electrical Engineering and Computer Applications (IEEE, 2021) 399–404. <https://doi.org/10.1109/AEECA52519.2021.9574221>
- 31 H. Zhao, X. Jiang, L. He, Y. Wu, F. Ai, X. Liang, and W. Li: 2022 IEEE Transportation Electrification Conf. and Expo, Asia-Pacific (IEEE, 2022) 1–6. <https://doi.org/10.1109/ITECA52519.2022.9942171>
- 32 B. G. Kim, F. P. Tredeau, and Z. M. Salameh: 2008 IEEE Vehicle Power and Propulsion Conf. (IEEE, 2008) 1–5. <https://doi.org/10.1109/VPPC.2008.4677513>
- 33 https://datasheet.lcsc.com/lcsc/HYCON-Tech-HY2213-BB3A_C113632.pdf (accessed January 2024).
- 34 <https://www.winson.com.tw/uploads/images/WCS1600.pdf> (accessed January 2024).

About the Authors



Rodi Hartono received his B.S. degree in electrical engineering from Universitas Komputer Indonesia, Indonesia, in 2010, and his M.S. degree in electrical engineering from Institut Teknologi Bandung, Indonesia, in 2014. Since 2021, he has been pursuing a Ph.D. degree at the Department of Artificial Intelligence Convergence, Busan University of Foreign Studies, Republic of Korea. (rodihartono@gmail.com)



Sang min Oh earned a bachelor's degree in mechanical engineering from Yeungnam University in 2018, graduated from Busan University of Foreign Studies in 2020 with a master's degree in creative convergence, and since 2020, he has been pursuing a doctorate degree in the Department of Artificial Intelligence Convergence at Busan University of Foreign Studies. (zkisszday@naver.com)



Sung Won Lim received her bachelor's degree from Busan University of Foreign Studies, Republic of Korea, in 2019. She received her master's degree from Busan University of Foreign Studies, Republic of Korea, in 2023. Since 2023, she has been pursuing her Ph.D. degree at the Department of Artificial Intelligence Convergence, Busan University of Foreign Studies. She has a strong interest in NLP and deep learning. (wonirosoida33@gmail.com)



Patrick Tshibang A Kalend received his bachelor's degree in computer science engineering, focusing on the field of information system engineering, from Université Protestante de Lubumbashi, Democratic Republic of Congo, in 2016. After his graduation, he presented lectures and led students in their projects for graduation. Since 2022, he has been pursuing his master's degree at the Department of Artificial Intelligence Convergence, Busan University of Foreign Studies. He has a strong interest in AI, computer vision, robotics, and IoT. (patricktshibang7@gmail.com)



Jasurbek Doliev is an undergraduate student in the Department of Artificial Intelligence Convergence, Busan University of Foreign Studies. He is a member of the Future Creative Science Research Institute at BUFS. He has a profound interest in AI, electrical engineering, robotics, image processing, IoT, battery pack designing, and clean energy. (dolievjasurbek0@gmail.com)



Jun Hyuk Lee is an undergraduate student in the Department of Artificial Intelligence Convergence, Busan University of Foreign Studies. He is a member of the Future Creative Science Research Institute at BUFS. He has a profound interest in AI, electrical engineering, robotics, image processing, and IoT systems. (happiness_1984@naver.com)



Kyoo Jae Shin is a professor of intelligent robot science at Busan University of Foreign Studies, South Korea. He is the director of the Future Creative Science Research Institute at BUFS. He received his B.S. degree in electronics engineering from Wonkwang University in 1985, his M.S. degree in electrical engineering from Cheonbuk National University in 1988, and his Ph.D. degree in electrical science from Pusan National University in 2009. Dr. Shin has been a professor at the Navy Technical Education School and the main director and research associate of dynamic stabilization systems at Busan Defense Weapon Research Institute. He has also researched and developed a fish robot, a submarine robot, an automatic dog spaying robot operating in a glass room, an automatic milking robot operated using a manipulator, a personal electrical vehicle, a smart accumulated aquarium using a heat pump, a solar tracking system, a 3D hologram system, and a gun/turret stabilization system. He is interested in intelligent robots, image signal processing application systems, smart farms, and aquariums using new energy and IoT technology. (kyoojae@bufs.ac.kr)